

UN MODELLO DI ELEMENTO FINITO PER L'ANALISI DI STRUTTURE
MURARIE SOGGETTE AD AZIONI CICLICHE

A FINITE ELEMENT MODEL FOR THE ANALYSIS OF MASONRY
STRUCTURES UNDER CYCLIC ACTIONS

U. Andreaus, M. Cerone, P. D'Asdia, F. Iannozzi

Istituto di Scienza delle Costruzioni, Facoltà di Ingegneria,
Università di Roma "La Sapienza", Via Eudossiana 18, 00184 ROMA

SOMMARIO

Scopo della nota proposta è di presentare un semplice modello matematico per l'analisi del comportamento di strutture murarie soggette ad azioni sia monotoni che sia cicliche.

Il modello consente di simulare le seguenti caratteristiche fondamentali, come sono mostrate dalle prove sperimentali:

- 1) una adeguata rappresentazione del dominio di resistenza ultimo;
- 2) una soddisfacente schematizzazione di ogni possibile percorso tensione-deformazione sotto carico monotono, prendendo in considerazione anche il ramo discendente;
- 3) una sufficiente capacità di descrivere il comportamento di elementi murari soggetti ad azioni cicliche severe tenendo conto della apertura e chiusura delle lesioni e del degrado del materiale.

SUMMARY

Aim of the proposed paper is to present a simple mathematical model for the analysis of masonry structure behaviour both under monotonic and cyclic loadings.

The model allows to simulate the following basic features, as they are shown by experimental tests:

- 1) an adequate representation of the ultimate strength domain;
- 2) a satisfactory schematization of every allowable stress-strain path under monotonic loading, taking into consideration the descent branch too;
- 3) a sufficient ability to describe masonry element behaviour under severe cyclic actions accounting for opening and closing of cracks and material degrading.

1. GENERALITIES

A finite element model for the analysis of masonry structures should allow to represent at least the following fundamental features of material, as they result from experimental investigation:

- 1) failure domains under single and combined stresses, like normal and shear stresses;
- 2) stress-strain paths for monotonically increasing loads as far as the ultimate strength is attained and the descendent branch is covered;
- 3) mechanical behaviour under severe cyclic loading at low cycle fatigue.

Special attention should be paid to evaluate the deterioration of mechanical characteristics, like strength and/or stiffness, of masonry both in the descendent branch of the stress-strain path under monotonically increasing loads and more generally in hysteretic loops under cyclic loading.

Masonry is a non-homogeneous and anisotropic material which may be discretized by using finite element techniques; Hrennikoff, (1), demonstrated through suitable examples the reliability of results obtainable by a discretization method based on truss-like systems, and Klingner and Bertero, (2), adopted two diagonal pin-jointed bars to simulate a masonry panel infilling a reinforced concrete frame.

The choice of the model depends on the type of analysis one intends to perform. Studying large structures or complicated members requires to represent global rather than local behaviour, provided all its fundamental features are adequately schematized.

Furthermore, a model should be well suitable for computer use, allowing the representation, within the same automatic program, of any type of material behaviour, from the simplest ones, like elastic or elastic - perfectly plastic, to more complicated ones accounting for structural damage, internal slippage and force release effects.

2. PRIMARY MODEL

A one-dimensional model has been formulated in (3); such model, of which Fig. 1 shows an extremely simplified version, but already sufficient to describe masonry behaviour in practical applications, can be assembled in a truss-like plane or space system, as shown in Fig. 2, in order to generate a sort of finite element, or "cell" whose behaviour defines the constitutive law and the failure domain of an ideal material representing real masonry by a suitable choice of the values given to the stiffnesses " k " and limit strengths " f " of the constituting truss members.

The typical features of the proposed model are listed below, which make it suitable for static and dynamic analysis of masonry structures.

2.1. Elastic behaviour

Identifying elastic stiffnesses of truss members allows to simulate elastic parameters of isotropic masonry, as well as an orthotropic material, like brick masonry.

With reference to this it is worth to be noticed that general purpose computer programs, widely used for numerical investigation of masonry, are unable to account for orthotropy even in elastic range, because they have been conceived for modelling concrete.

As an example, the relationships between the elastic characteristics of the truss members constituting the plane "cell" of Fig. 2a ($k_v^+, k_v^-, k_d^+, k_d^-, k_o^+, k_o^-$), and the actual ones of masonry ($E_x, E_y, \nu_x, \nu_y = \nu_x E_y/E_x$) are given in the following:

$$k_d^+ = k_d^- = k_d,$$

$$k_d = 2s/\sin 2\beta \cdot G_{xy} G_{yx} / (G_{xy} + G_{yx}),$$

$$k_v^+ = \frac{1}{2} (a/b) s E_y - k_d \sin \beta (\sin \beta - \nu_x (a/b) \cos \beta),$$

$$k_v^- = (k_d / \nu_y) (a/b) \sin \beta (\cos \beta - \nu_y (b/a) \sin \beta),$$

$$k_o^+ = \frac{1}{2} (b/a) s E_x - k_d \cos \beta (\cos \beta - \nu_y (b/a) \sin \beta),$$

$$k_o^- = (k_d / \nu_x) (b/a) \cos \beta (\sin \beta - \nu_x (a/b) \cos \beta).$$

2.2. Failure domains

The suitable choice of limit elastic strengths of single truss members comprising the finite element model allows to obtain failure domains which satisfactorily approximate those ones of masonry, (4, 5). In particular, as far as the plane "cell" of Fig. 2a is concerned, the failure domain under normal stresses N_x and N_y acting along the orthotropy axes can be modelled as shown in Fig. 3. For this domain, as an example, the relationships between limit forces of truss members (f_v^+ , f_v^- , f_d^+ , f_d^- , f_o^+ , f_o^-) and limit values of N_x and N_y which characterized the domain, read as follows:

$$f_o^+ = N_x^2 - f_d^+ \sin \beta$$

$$f_o^- = N_x^2 - f_d^- \sin \beta$$

$$f_v^+ = N_y^2 - f_d^+ \cos \beta$$

$$f_v^- = N_y^2 - f_d^- \cos \beta$$

$$N_x^4 = -N_x^1 + (f_d^+ + f_d^-) \sin \beta$$

$$N_x^3 = N_x^2 - (f_d^+ + f_d^-) \sin \beta$$

$$N_y^4 = -N_y^1 + (f_d^+ + f_d^-) \cos \beta$$

$$N_y^3 = N_y^2 - (f_d^+ + f_d^-) \cos \beta$$

Figure 4 represents the failure domain under biaxial normal stress N_x , N_y , and shear stress T , according to the previously identified parameters.

The same domain is represented by contour lines in Fig. 5a. The edge solid line represents the failure domain under biaxial stress state, N_x-N_y . Section A-A of the domain in Fig. 5a is depicted in Fig. 5b, which represents the failure domain N_x-T at $N_y = \text{const.}$ The dashed line in the same figure is the domain at $N_y=0$.

3. IMPROVEMENT OF THE PRIMARY MODEL

Figure 6a shows, for the primary model of Sect.2, the behaviour of the "cell" in the biaxial normal stress domain for different load paths represented in the force-displacement diagrams of Fig. 6b; the dashed line in Fig. 6a bounds the elastic domain. It is worthwhile noticed that, even if the elastic domain does not coincide with the limit one, the bi-linear behaviour of the single truss members induces a quasi-bi-linear behaviour of the "cell" as a whole.

Thus it stands to reason that, by defining more refined force-displacement diagrams for the single truss members, it is possible to achieve a better approximation of the model behaviour to the actual one of masonry, especially under cyclic loading.

Figure 7 shows the simplest schematization of the masonry behaviour under monotonically increasing uniaxial deformation. Branch A' OA represents the elastic range; points A and A' define the ultimate strengths in tension and compression respectively; the descendent branch of the force-deformation path is approximated by a straight line.

If local unloading occurs in B, the slope of the unloading path equals the initial one (branch OA), as far as the force sign changes in C. Branch OC represents the irreversible deformation due to material crushing.

If the force becomes negative the diagram exhibits a branch CD parallel to OA'. Material fails in tension at point D and a crack of amplitude CD' instantaneously takes place. Henceforth masonry strength in tension permanently drops out; any further decrement of deformation enlarges the crack amplitude covering the branch D'E; a subsequent deformation increment can shut the crack covering the branch EC at $f=0$. A further deformation increment covers the reloading branch CB and, subsequently, the descending branch BB*. A possible unloading branch B* C* goes on δ -axis since the tensile strength has dropped out.

Dissipated energy in the first cycle O A B C D D' E O is given by areas O A B C, C D D', and in the second cycle by C B B* C*.

It is worth noticing that there is non superposition of areas representing dissipated energy; therefore dissipated energy is given by the areas A B B_{lim} C_{lim}, as well as by the very small one given by the triangle which can be covered only once in tension.

The above described model behaviour can be refined in order to better approximate some experimental results.

A first improvement consists in introducing a parameter α which allows to take into account that cracks, after an opening stage (branch CE of δ -axis), when a deformation reversal occurs (path E C) shut before or after point C.

Closing at point C₁ on the "left" of C denotes an indentation effect at crack's edges; therefore the two crack's faces do not coincide any longer, due to interposing of residual material or to small relative displacements. On the contrary, opening of C₁ on the "right" of C indicates ejection of material due to crack opening. The two above mentioned cases can be unified by posing $\overline{EC}_1 = \alpha \overline{EC}$, where α is less or greater than unity respectively. If α is less than unity material still exhibits an hysteretic loop and hence dissipated energy increases with respect to the above described case $\alpha = 1$ (see Fig. 8a). Viceversa, if α is greater than unity dissipated energy decreases (see Fig. 8b).

The schematization of the descendent branch of strength in compression can be improved by a multi-linear approximation.

Moreover, introducing a damage parameter, which depends on maximum deformation and/or dissipated energy, (3), and affects the moduli $k_1 = \tan \varphi_1$ and $k_2 = \tan \varphi_2$, allows to account for stiffness deterioration in unloading and reloading pa-

ths, as shown by experimental results; in this way too the force-deformation curve can be schematized by a multi-linear approximation, as shown in Fig. 9.

The equality $f(B_1) = f(B)$ is enforced for $\alpha < 1$; for $\alpha > 1$, B_1 is enforced to lie on the branch moving from B.

Thus, for $\alpha < 1$, the model exhibits an hardening or softening effect respectively if $\varphi_2 > 0$ or $\varphi_2 < 0$ at the stress point.

4. MODELLING OF MASONRY PANELS

Identifying stiffnesses and strengths of the single truss members comprising the "cell" allows to study the behaviour of structural members by means of few or even only one finite element, provided only global stress-strain paths and failure domains are required to be known.

As an example, the behaviour of a square masonry panel (2ax2a) under horizontal and vertical eccentric pressures, as shown in Fig. 10, can be simulated by means of only one "cell".

The corresponding failure domains of the isotropic panel are depicted in Fig. 11.

Obviously analysing local stress and strain states or complicated geometrical and loading conditions require a more refined discretization, which has been adopted to work out some sample applications of the proposed method.

4.1. Square panel under monotonically increasing vertical load.

Two support conditions are considered. In the first one (see Fig. 12) horizontal strains are prevented at upper and lower edges; in the second one (Fig. 13) horizontal fibres at the contact surfaces can freely stretch.

The collapse mechanisms and the relevant ultimate loads are given in the same figures, where P_0 is the ultimate mono-axial strength of the panel.

It is interesting to be noticed that numerical experimentation on the basis of the proposed model adequately simulates, even by a roughly discretization, actual well known failure mechanisms.

4.2. Square panel under horizontal and vertical monotonically increasing loads.

The same panel of sect. 3.1. has been subjected to the support conditions of Figs. 8 and 9 and to lateral confinement. Figure 14 shows the three corresponding failure domains under the vertical load P and the horizontal force H . Comparing the three diagrams stresses the importance of support conditions, which influence the collapse mechanism. It is worthwhile noticed that some of the more widely known expressions which give the shear strength of masonry, based on the Mohr-Coulomb law, provides qualitatively similar curves.

4.3. Three-story wall

The masonry wall shown in Fig. 15a exhibits 90x90 cm windows. Each storey panel, having length 10.8 m, height 2.7 m, thickness respectively 50, 40, 30 cm, has been discretized by 35 square "celles", while the influence of slabs, with the relevant edge beams, has been simulated at each floor by means of 12 truss-like systems, whose stiffness is much larger than masonry's one.

The wall has been subjected first to vertical forces equal to the dead loads of the wall itself and of the edge beams, and secondly to three horizontal forces linearly distributed along the height, which are statically equivalent to a seismic action and monotonically increasing up to failure.

The curves shown in Fig. 15b represents the load factor versus the horizontal displacement of the third floor. At $\lambda = 1$ the horizontal forces have the following reference values: $F_3 = 30. \text{ t}$, $F_2 = 20. \text{ t}$, $F_1 = 10. \text{ t}$. Figure 16 gives the deformed shapes of the wall under vertical and horizontal loads respectively; displacements have been amplified 1000-times in the first case and 100-times in the second case; figure 16b shows ground normal stress distribution.

5. MASONRY PANEL UNDER CONSTANT VERTICAL LOAD AND CYCLIC HORIZONTAL FORCE

The masonry panel under investigation and the corresponding model are shown in Figure 17.

Figure 18 represents structural response in the first loading cycles.

Comparing model response with recent experimental results, (6), given in Fig. 19, proves the reliability of the proposed model; obviously a more refined discretization allows to more strictly approximate the experimental results.

6. REFERENCES

- (1) Hrennikoff A., "Precision of finite element method in plane stress", Proc. of IABSE, Vol. 29-II, Zürich, 1969, pp. 125-137.
- (2) Klingner R.E., Bertero V. V. "Earthquake resistance of infilled frames", J. of the Struct. Div., ASCE, Vol. 104, No. ST6, June 1978, pp.
- (3) Andreus U., G. Ceradini, P. D'Asdia, "A simple model for the dynamic analysis of deteriorating structures", Proc. of the 7-th Int. Conf. on Structural Mechanics in Reactor Technology, Chicago, August 22-26, 1983, Vol. L., pp. 591-598.
- (4) Page A. W., "A biaxial failure criterion for brick masonry in the tension-tension range", Int. J. of Masonry Construction, 1980, Vol. I, No. 1, pp. 26-29.
- (5) Page A. W., "An experimental investigation of the biaxial strength of brick masonry", 6-th IBM aC, Rome, 1982, pp. 3-15.
- (6) Benedetti D., Binda L. et al., "Static and seismic behaviour of masonry structures", Ed. CLUP, Milan, 1982.

Fig. 1

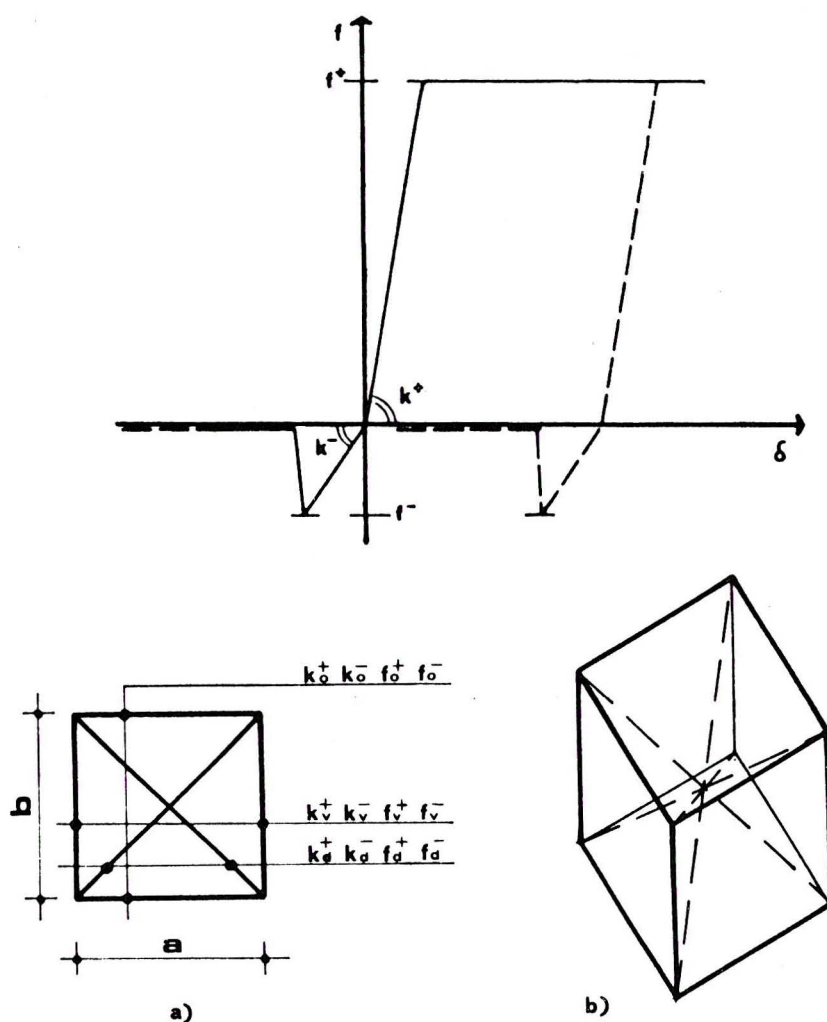


Fig. 2

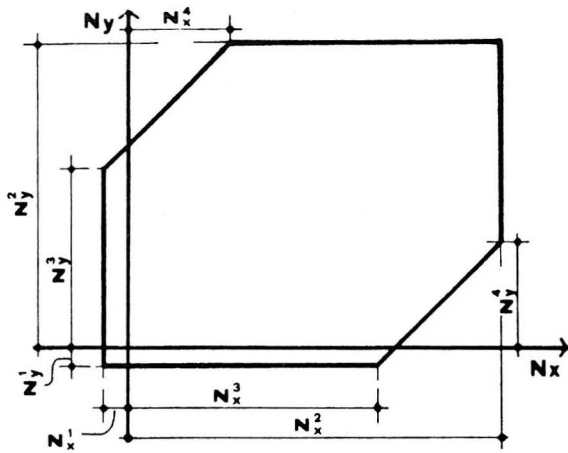


Fig. 3

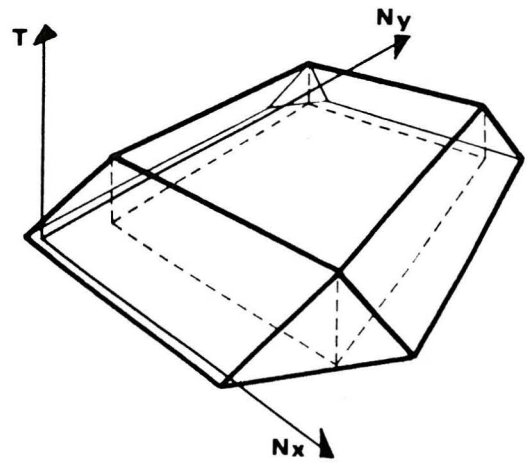


Fig. 4

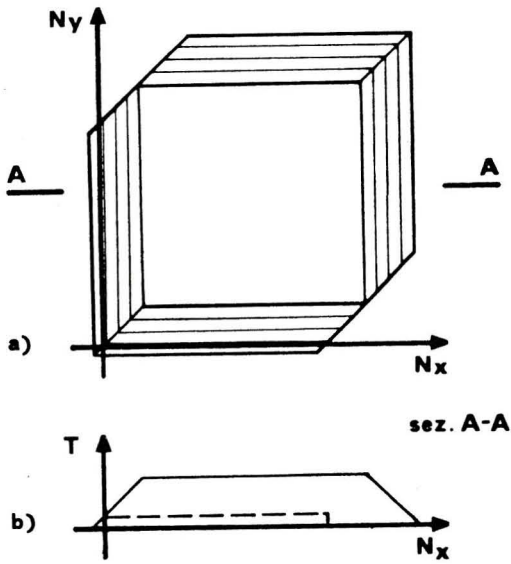


Fig. 5

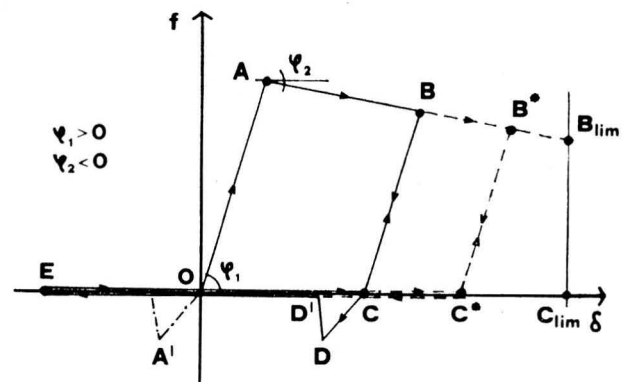
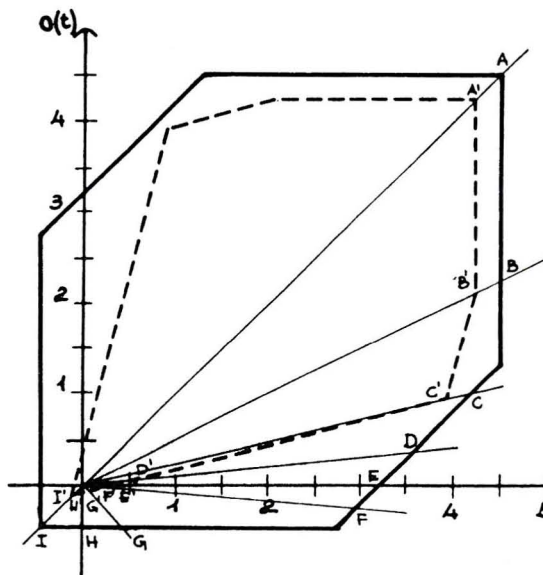
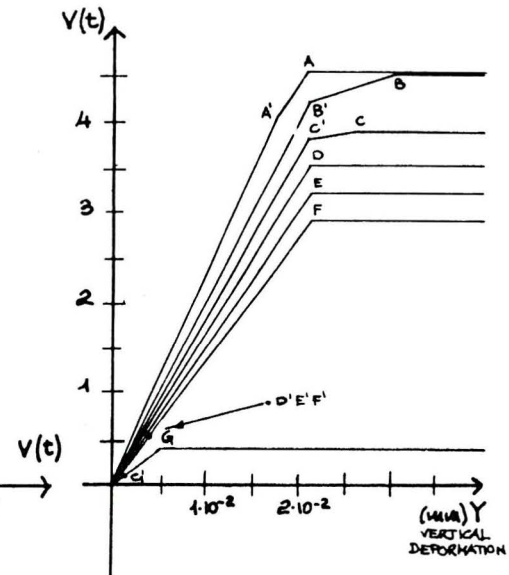


Fig. 6



$$\begin{aligned}
 k_v^+ &= k_v^- = 744.050 \text{ kg/cm} \\
 k_o^+ &= k_o^- = 744.050 \text{ kg/cm} \\
 k_d^+ &= k_d^- = 365.630 \text{ kg/cm}
 \end{aligned}$$

a)



$$\begin{aligned}
 f_v^+ &= 1550 \text{ kg} & f_v^- &= 25 \text{ kg} \\
 f_o^+ &= 1550 \text{ kg} & f_o^- &= 25 \text{ kg} \\
 f_d^+ &= 386 \text{ kg} & f_d^- &= 282 \text{ kg}
 \end{aligned}$$

b)

Fig. 7

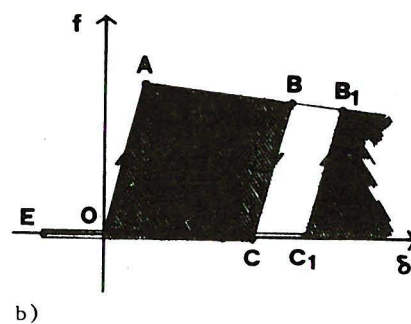
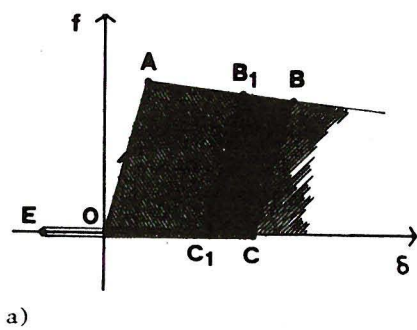


Fig. 8

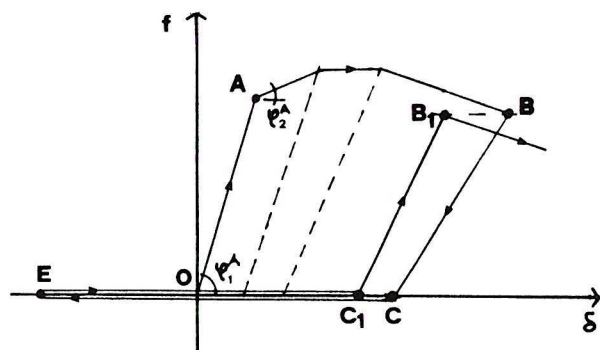


Fig. 9

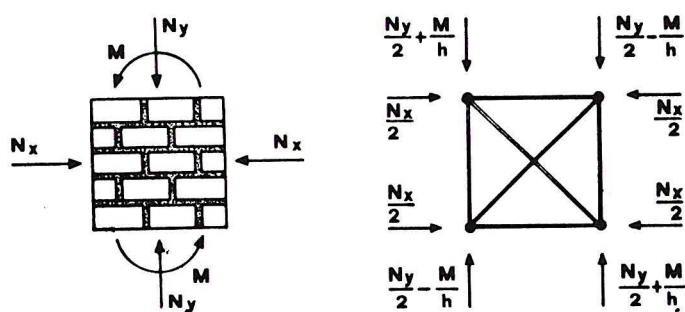


Fig. 10

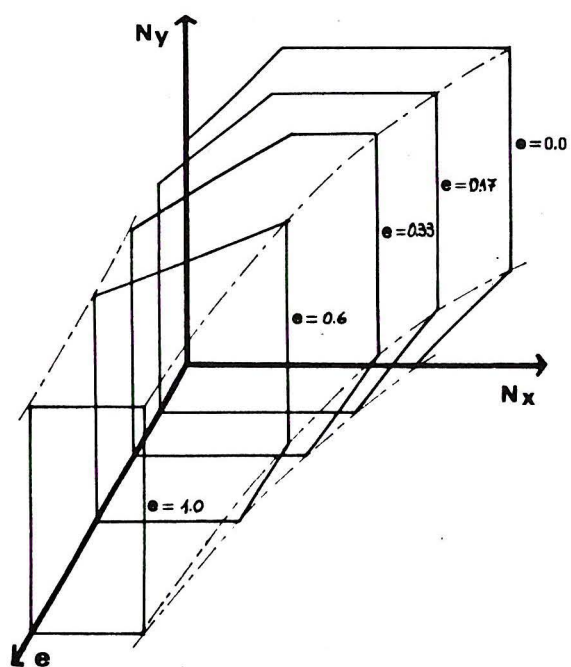
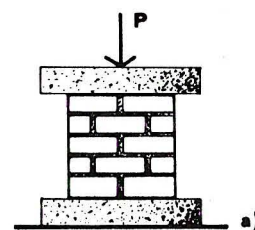


Fig. 11



$$P_{\max} = 1.17 P_0 = 19.6 \text{ t}$$

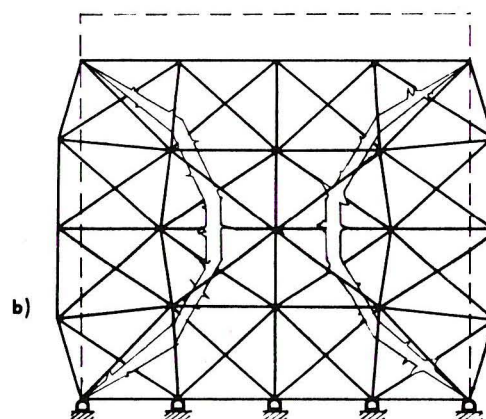


Fig. 12

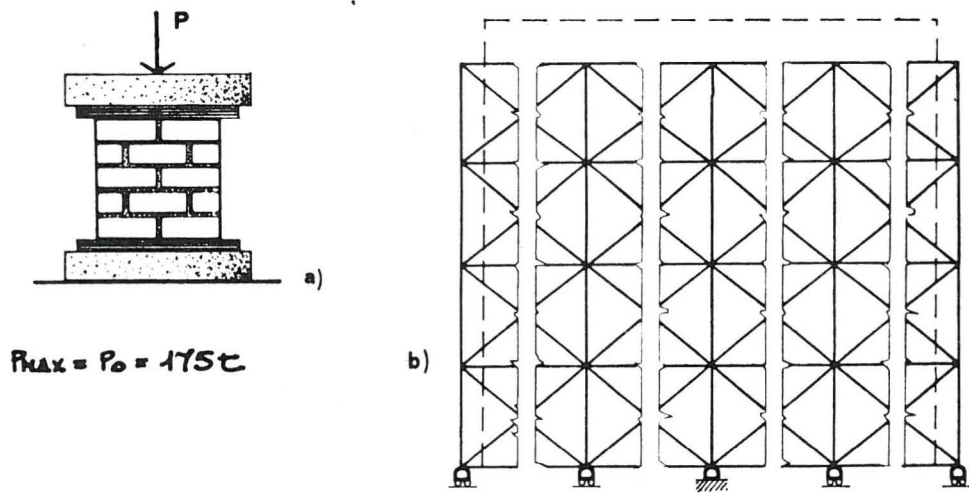


Fig. 13

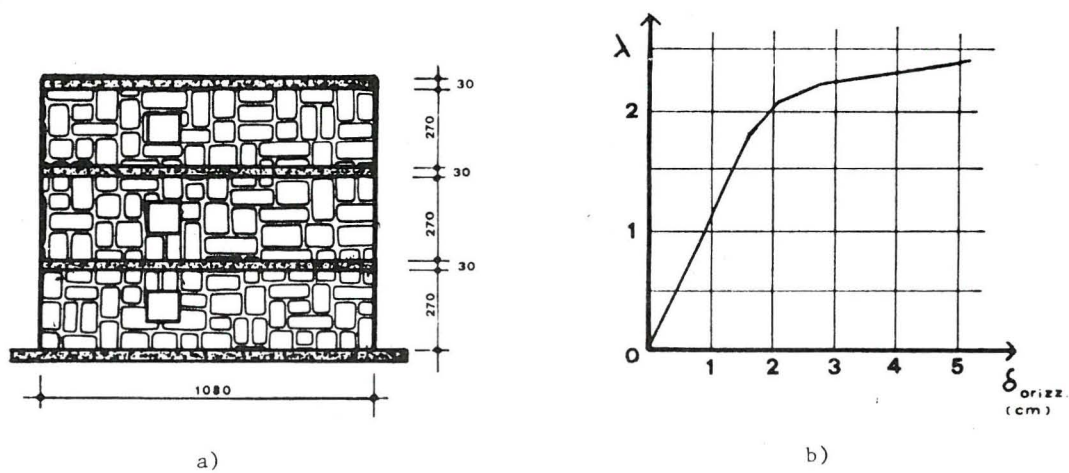
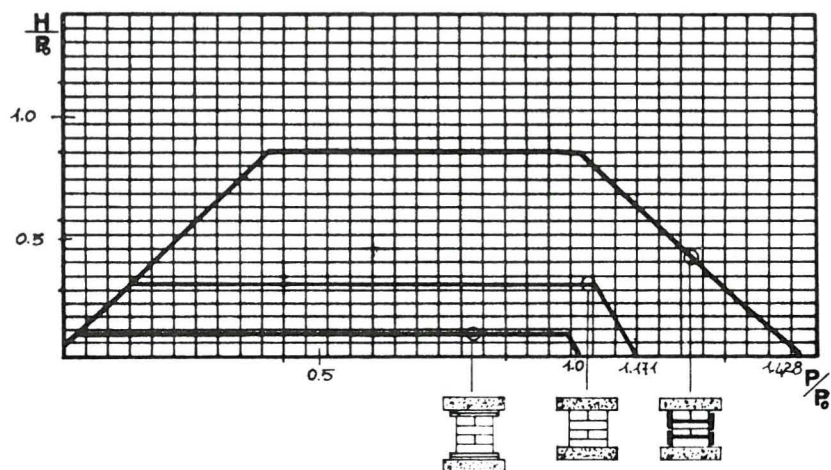


Fig. 15

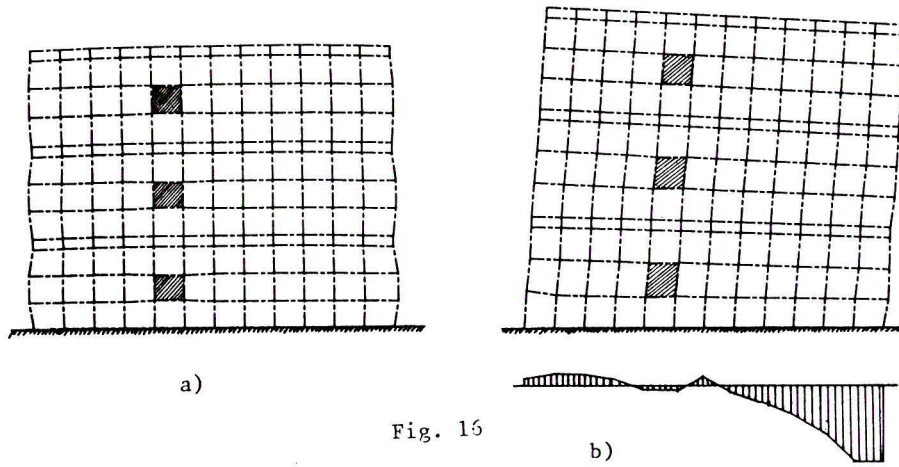


Fig. 16

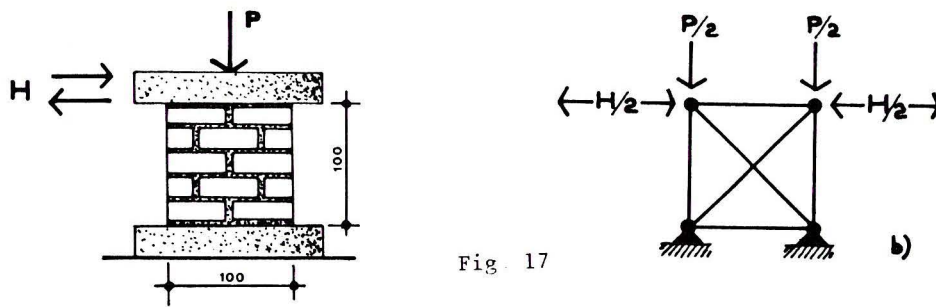


Fig. 17

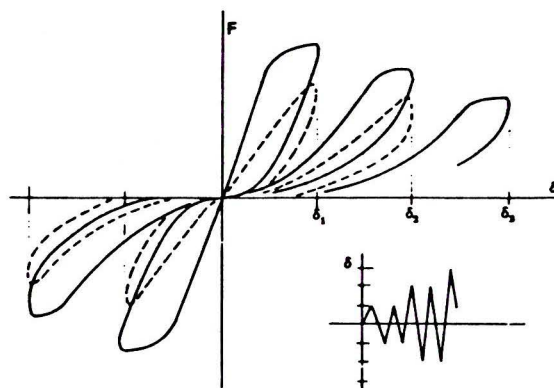
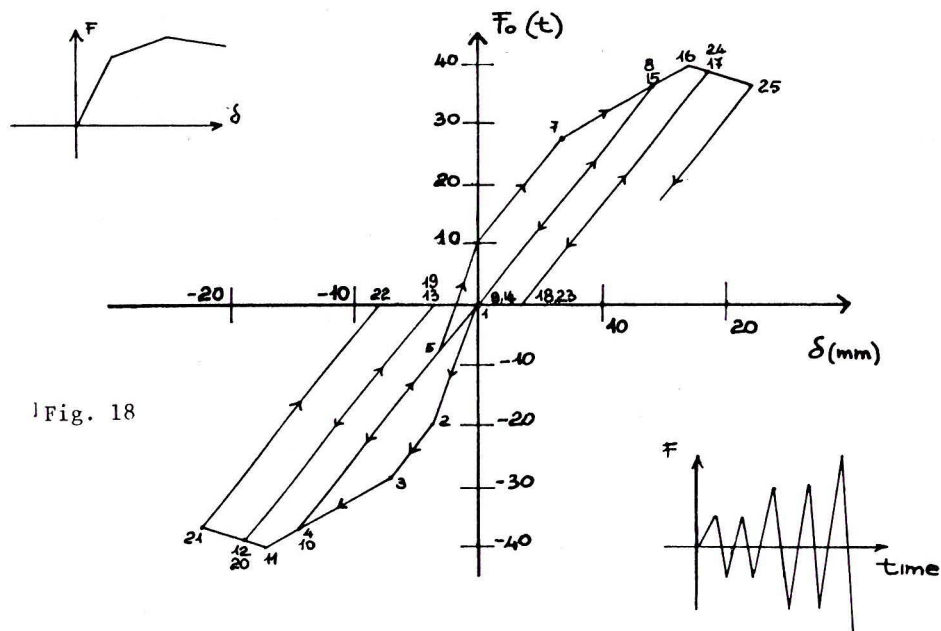


Fig. 19